

Theoretical Study of Benzotriazole UV Photostability: Ultrafast Deactivation through Coupled Proton and Electron Transfer Triggered by a Charge-Transfer State

Martin J. Paterson,[†] Michael A. Robb,^{*,†} Lluis Blancafort,^{*,‡} and Anthony D. DeBellis[§]

Contribution from the Department of Chemistry, Imperial College London, London, SW7 2AZ, United Kingdom, Institut de Química Computacional, Departament de Química, Universitat de Girona, Campus de Montilivi, 17071 Girona, Spain, and Ciba Specialty Chemicals, Coating Effects Research Department, 540 White Plains Road, Tarrytown, New York 10591

Received September 22, 2003; E-mail: mike.rob主@imperial.ac.uk; lluisb@stark.udg.es

Abstract: A theoretical CASSCF study of the reaction path for excited-state intramolecular proton transfer (ESIPT) for a model system derived from the UV absorber 2-(2'-hydroxyphenyl) benzotriazole without the fused benzo ring on the triazole has been carried out. A planar reaction path can be optimized but is shown to have no physical significance. The true reaction path involves twisted geometries. Adiabatic proton transfer is triggered by a charge-transfer from the phenol to the triazole group, and is followed by radiationless decay at the keto form. Along the nonplanar reaction path, there is a coupled proton and electron transfer in a manner similar to tryptophan. This rationalizes unexpected experimental results on the effect of electron withdrawing substituent groups on the photostability. The coupled proton and electron transfer is followed by a barrierless relaxation in the ground state to recover the enol form. An alternative photostabilization pathway from a phenyl localized state has also been documented and is similar to the channel 3 decay pathway in benzene photochemistry. Additionally, a long-lived intermediate for a twisted intramolecular charge-transfer (TICT) state has been identified as the species potentially responsible for the increase of blue fluorescence in strongly polar media.

Introduction

Orthohydroxyphenyl benzotriazoles are compounds that are commonly used as ultraviolet absorbers.¹ They absorb potentially destructive UV radiation and dissipate the energy on a subpicosecond time scale.^{1–6} The absorber is used to filter off UV radiation and dissipate the energy in the form of heat i.e., generate a thermally excited ground-state species. UV absorbers must have a wide range of chemical and physical properties to be useful in applications, which include coatings and a wide variety of polymer products.¹ An essential property of UV absorbers is that they possess a mechanism for the rapid dissipation of the absorbed UV radiation via some suitable intramolecular rearrangement.

For the benzotriazole class of UV absorbers, the mechanism of excited-state deactivation is thought to be due to an excited-state intramolecular proton transfer (ESIPT).^{1–7} This is also thought to be the decay mechanism for other photostabilizers such as hydroxyphenyl triazines.⁴ Such molecules contain a strong intramolecular hydrogen bond in the ground state, which is believed to be essential for the photostability of these compounds.^{1–6} The fact that benzotriazole photodeactivation occurs on an ultrafast time scale suggests the involvement of conical intersections on the intramolecular proton-transfer reaction path.^{8–12} Conical intersections can act as efficient decay funnels leading from the excited state to the ground state within a single vibrational period and are ubiquitous throughout ultrafast photochemistry and photophysics.^{10–17}

[†] Department of Chemistry, Imperial College London.

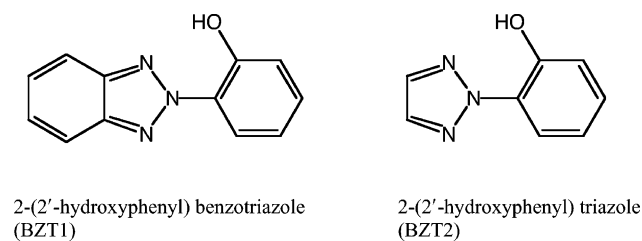
[‡] Institut de Química Computacional, Departament de Química, Universitat de Girona.

[§] Ciba Specialty Chemicals, Coating Effects Research Department.

- (1) Leppard, D.; Hayoz, P.; Schäfer, T.; Vogel, T.; Wendeborn, F. *Chimia* **2002**, *56*, 216–224.
- (2) Stein, M.; Keck, J.; Waiblinger, F.; Flugge, A. P.; Kramer, H. E. A.; Hartsmuch, A.; Port, H.; Leppard, D.; Rytz, G. *J. Phys. Chem. A* **2002**, *106*, 2055–2066.
- (3) Maliakal, A.; Lem, G.; Turro, N. J.; Ravichandran, R.; Suhadolnik, J. C.; DeBellis, A. D.; Wood, M. G.; Lau, J. *J. Phys. Chem. A* **2002**, *106*, 7680–7689.
- (4) Waiblinger, F.; Keck, J.; Stein, M.; Flugge, A. P.; Kramer, H. E. A.; Leppard, D. *J. Phys. Chem. A* **2000**, *104*, 1100–1106.
- (5) Suhadolnik, J. C.; DeBellis, A. D.; Hendricks-Guy, C.; Iyengar, R.; Wood, M. G. *J. Coat. Technol.* **2002**, *74*, 55.
- (6) McGarry, P. F.; Jockush, S.; Fujiwara, Y.; Kaprinidis, N. A.; Turro, N. J. *J. Phys. Chem. A* **1997**, *101*, 764–767.

- (7) Estevez, C. M.; Bach, R. D.; Hass, K. C.; Schneider, W. F. *J. Am. Chem. Soc.* **1997**, *119*, 5445–5446.
- (8) Blancafort, L.; Gonzalez, D.; Olivucci, M.; Robb, M. A. *J. Am. Chem. Soc.* **2002**, *124*, 6398–6406.
- (9) Ismail, N.; Blancafort, L.; Olivucci, M.; Kohler, B.; Robb, M. A. *J. Am. Chem. Soc.* **2002**, *124*, 6818–6819.
- (10) Michl, J.; Bonacic-Koutcky, V. *Electronic Aspects of Organic Photochemistry*; Wiley: New York, 1990.
- (11) Klessinger, M.; Michl, J. *Excited States and Photochemistry of Organic Molecules*; VCH: New York, 1994.
- (12) Blancafort, L.; Ogliaro, F.; Olivucci, M.; Robb, M. A.; Bearpark, M. J.; Sinicropi, A. In *Computational Methods in Photochemistry*; Kutateladze, A., Ed.; Marcel Dekker: New York, 2004.
- (13) Robb, M. A.; Garavelli, M.; Olivucci, M.; Bernardi, F. *Rev. Comput. Chem.* **2000**, *15*, 87–146.
- (14) Sanchez-Galvez, A.; Hunt, P.; Robb, M. A.; Olivucci, M.; Vreven, T.; Schlegel, H. B. *J. Am. Chem. Soc.* **2000**, *122*, 2911–2924.

Scheme 1



Given the commercial importance of ultraviolet absorbers, the mechanism of the ESIPT and subsequent radiationless decay has been studied experimentally (see refs 2–6 for most recent work) and theoretically,⁷ although the details are far from clear. These previous studies suggest that the reaction coordinate for the radiationless deactivation process is probably more complicated than a simple proton transfer with a planar transition state. Previous computations on several model chromophore systems⁷ have strongly suggested the role of conical intersections in the decay, and they pointed out the importance of charge-transfer from the phenol ring to the triazole ring and of the folding of the keto form.⁷ As we shall discuss subsequently, our computations, support these conclusions. Moreover, we have explored the full reaction coordinate, including the excited-state proton transfer and the regeneration of the enol during the radiationless decay. As we show below, we have been able to relate our results to experimental data and we provide alternative mechanisms for the neutral chromophore and its deprotonated form.

The model used in our study of the proton-transfer reaction is an analogue of 2-(2'-hydroxyphenyl) benzotriazole (BZT1), lacking the fused benzo ring, 2-(2'-hydroxyphenyl) triazole (BZT2) (see Scheme 1). We have calibrated BZT2 by computing the vertical excitation energies of BZT1 and BZT2 with time-dependent density functional theory (TD-DFT) and complete active space self-consistent field (CASSCF) theory. As we discuss below, our study of the BZT2 model at the CASSCF level implies some shortcomings, because we are effectively ignoring a local excitation on the benzotriazole moiety of BZT1 and our calculations lack dynamic correlation. However, with the present methodology we have been able to carry out a thorough investigation of the ESIPT coordinate, which overwhelmingly dominates the excited-state reactivity, and also to study several alternative paths.

The essential features of our computed reaction path for ESIPT are summarized in Figures 1 and 2, with the energetics given in Tables 1–3. Figure 1 shows the idealized reaction path for the lowest energy $n\pi^*$ state subject to a constraint of planarity, whereas the reaction path depicted in Figure 2 involves fully optimized structures without any constraint. The $n\pi^*$ state planar reaction path (Figure 1) has no physical meaning because a $\pi\pi^*$ state lies at lower energy at all points along the reaction path, so radiationless deactivation to the ground state is impossible. When the constraint of planarity is removed (see Scheme 2 and Figure 2), there are two decay pathways that involve a charge-transfer (CT) state from the phenol to the triazole group, and a locally excited state on the phenol moiety,

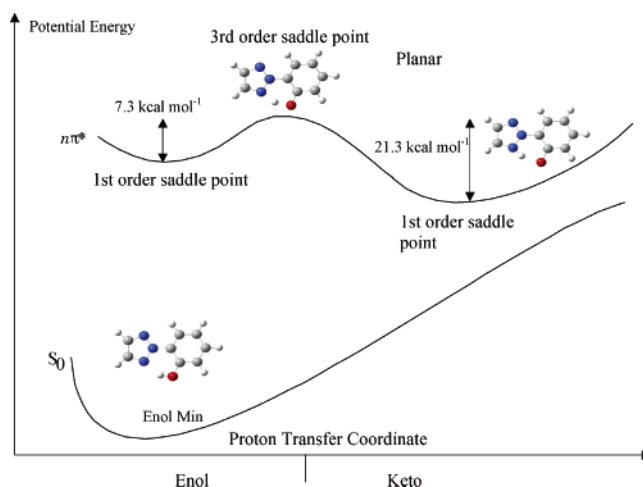


Figure 1. Potential energy profiles for ground and $n\pi^*$ states with the geometry constrained to be planar. Geometries given in Supporting Information (Energies relative to 3rd order saddle-point).

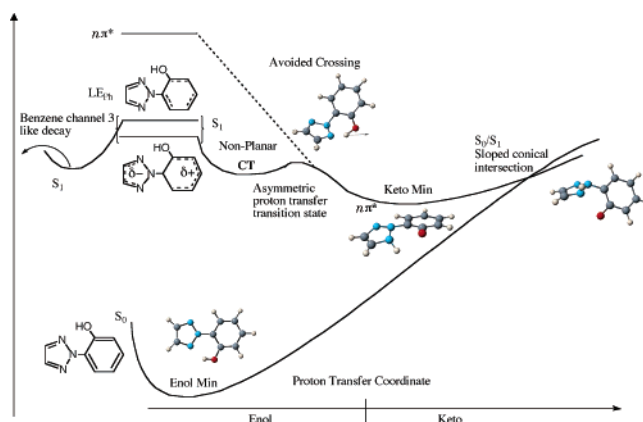


Figure 2. Schematic representation of the ground and $n\pi^*$ excited-state potential energy surfaces along the proton-transfer coordinate in the full space of nuclear coordinates. The reaction pathway involves an intertwining of the three excited states and the ground state. Geometries given in Table 4.

respectively (see the valence bond representation of these states in Figure 3). The main deactivation path (path A) is the ESIPT one and starts with formation of a nonplanar minimum of the enol form. The minimum corresponds to the CT state and is an excited-state complex with a strong hydrogen bond between the hydroxy group and the triazole hydrogen acceptor. The next step in path A is the tautomerization from the enol to the keto form of BZT. The tautomerization is associated with an avoided crossing and a state switch between the CT $\pi\pi^*$ state and a rapidly descending $n\pi^*$ state. The final step of this mechanism is decay to the ground state via a conical intersection of the keto tautomer that quickly regenerates the enol form. In fact our proposed mechanism, as we discuss below, explains several experimental results. From the mechanistic point of view, the coupled electron and proton transfer is a key feature of this type of decay mechanism, and we draw the analogy to the photochemistry of tryptophan⁸ in the next section.

The second path, path B, involves a planar enol-type minimum on the surface of S_1 , where the excitation is localized on the phenol moiety of BZT. The path goes through a conical intersection between the locally excited $\pi\pi^*$ state and S_0 , similar to the one found in the channel 3 decay of benzene. The deactivation from the locally excited phenyl $\pi\pi^*$ state can also

(15) Garavelli, M.; Bernardi, F.; Olivucci, M.; Vreven, T.; Klein, S.; Celani, P.; Robb, M. A. *Faraday Discussions* **1998**, *110*, 51–70.

(16) Bernardi, F.; Olivucci, M.; Robb, M. A. *Chem. Soc. Rev.*, **1996**, *25*, 321.

(17) Paterson, M. J.; Hunt, P. A.; Robb, M. A.; Takahashi, O. *J. Phys. Chem. A*, **2002**, *106*, 10 494–10 504.

Scheme 2

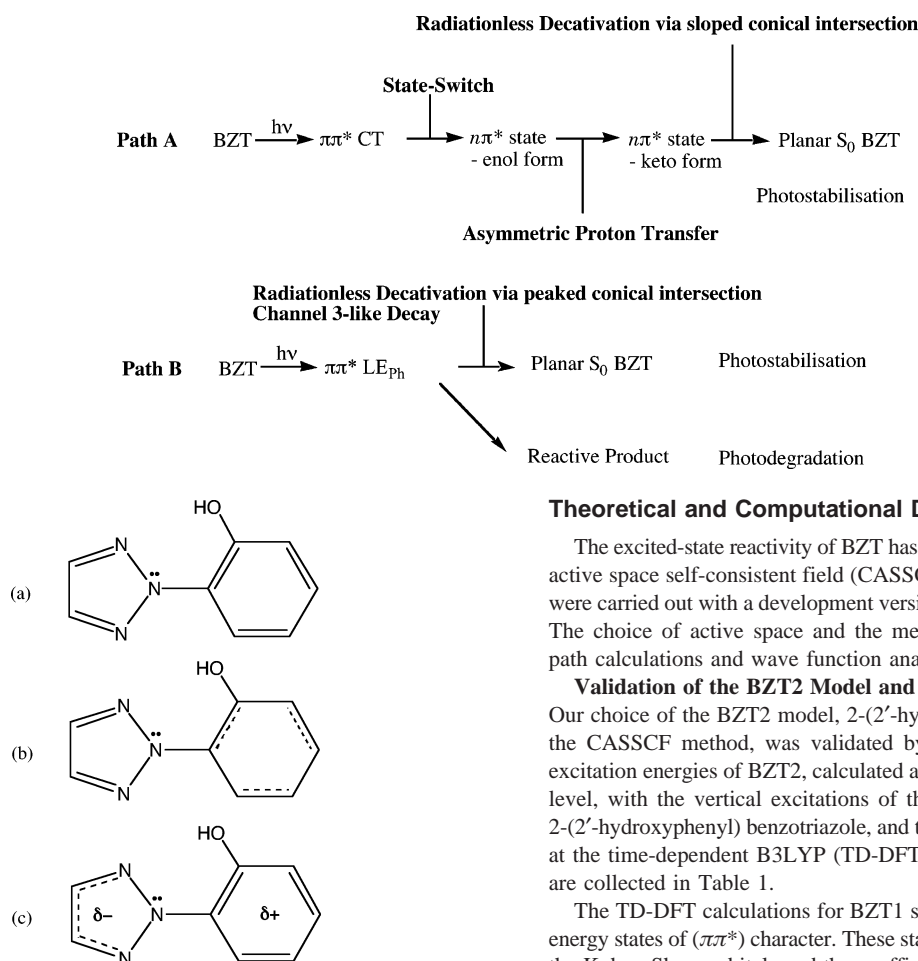


Figure 3. Valence-bond representation of CASSCF states as obtained from the spin-exchange densities given in Table 6. (a) Ground state, (b) Locally excited phenyl state, and (c) Charge-transfer state.

lead to a rearrangement of the benzene skeleton and possibly subsequent photodegradation.

In benzene photochemistry, the quantum yield of the reactive photochemical event (i.e., the production of prefulvene) is very small (~ 0.02). Thus, the majority of passes through the S_1/S_0 intersection simply regenerate the ground state reactants. The decay from the locally excited phenyl $\pi\pi^*$ state in BZT should be similar. Thus in the BZT2 model, this feature may account for the slight photodegradation which occurs over a significant period of time (i.e., after many photocycles).

The overall photostability problem is thus very complex involving the coupling of 4 electronic states via several nuclear degrees of freedom. We detail our results in the following stages: (1) A thorough analysis of the vertically excited states using TD-DFT and large active space CASSCF (using the spin-exchange density), (2) an examination of the hypothetical planar ES IPT reaction path, which we show to have no physical relevance, (3) a detailed discussion of the excited-state potential surfaces in the full space of nuclear coordinates, which reveals two possible pathways, and (4) an exploration of the excited-state potential surface of the phenolate anion BZT model that supports the proposal, based on experimental studies,³ that the enhanced fluorescence in the blue spectral range observed in DMSO arises from a long-lived, twisted intramolecular charge-transfer (TICT) state.¹⁸

Theoretical and Computational Details

The excited-state reactivity of BZT has been studied using a complete active space self-consistent field (CASSCF) formalism. Computations were carried out with a development version of the Gaussian program.¹⁹ The choice of active space and the methodologies for the reaction-path calculations and wave function analysis are discussed below.

Validation of the BZT2 Model and the CASSCF Methodology. Our choice of the BZT2 model, 2-(2'-hydroxyphenyl) triazole, and of the CASSCF method, was validated by comparison of the vertical excitation energies of BZT2, calculated at the CASSCF(14,12)/6-31G* level, with the vertical excitations of the complete BZT1 molecule, 2-(2'-hydroxyphenyl) benzotriazole, and the BZT2 analogue, calculated at the time-dependent B3LYP (TD-DFT) level of theory. The results are collected in Table 1.

The TD-DFT calculations for BZT1 show the presence of four low energy states of ($\pi\pi^*$) character. These states can be characterized using the Kohn–Sham orbitals and the coefficients of CIS-type excitations. In BZT1, Table 1, two of the excited states can be assigned as charge-transfer states, CT_1 and CT_2 , where the charge-transfer is from the phenol (from homo and homo-1, respectively) to the benzotriazole moiety. The remaining two states are locally excited-states, LE_{Ph} and LE_{Tz} , where the excitation is localized on the phenol and the benzotriazole moieties, respectively. The calculated oscillator strengths show that the three lowest-lying states (CT_1 , LE_{Tz} , and CT_2), are the main spectroscopically active states ($f > 0.10$), and the lowest-lying $n\pi^*$ state is S_5 (1.7 eV above S_1). Overall, the TD-DFT results are in very good agreement with the absorption spectrum of Tinuvin-P (a commercial derivative of BZT1) in C_2Cl_4 .²⁰ The lowest observed band at approximately 345 nm (3.59 eV) would thus correspond to the calculated CT_1 excitation. The fact that this is a CT state is confirmed experimentally where upon methylation of the hydroxyl group there is a decrease in the long wavelength absorption at 345 nm.²¹ The second observed band at around 300 nm (4.13 eV) would be the result of the overlapping LE_{Tz} and CT_2 bands.

(18) Rettig, W. *Topics Curr. Chem.* **1994**, *169*, 253–299.

(19) Frisch, M. J.; Trucks, G. W.; Schlegel, H. B.; Scuseria, G. E.; Robb, M. A.; Cheeseman, J. R.; Zakrzewski, V. G.; Montgomery, J. A.; Stratmann, R. E.; Burant, J. C.; Dapprich, S.; Millam, J. M.; Daniels, A. D.; Kudin, K. N.; Strain, M. C.; Farkas, O.; Tomasi, J.; Barone, V.; Cossi, M.; Cammi, R.; Mennucci, B.; Pomelli, C.; Adamo, C.; Clifford, S.; Ochterski, J.; Petersson, G. A.; Ayala, P. Y.; Cui, Q.; Morokuma, K.; Malick, D. K.; Rabuck, A. D.; Raghavachari, K.; Foresman, J. B.; Cioslowski, J.; Ortiz, J. V.; Stefanov, B. B.; Liu, G.; Liashenko, A.; Piskorz, P.; Komaromi, I.; Gomperts, R.; Martin, R. L.; Fox, D. J.; Keith, T.; Al-Laham, M. A.; Peng, C. Y.; Nanayakkara, A.; Gonzalez, C.; Challacombe, M.; Gill, P. M. W.; Johnson, B. G.; Chen, W.; Wong, M. W.; Andres, J. L.; Head-Gordon, M.; Replogle, E. S.; Pople, J. A. *Gaussian 98*, revision C.1, Gaussian, Inc., Pittsburgh, PA, **1998**.

(20) Wiechmann, M.; Port, H.; Frey, W.; Lärmer, F.; Elsässer, T. *J. Phys. Chem.* **1991**, *95*, 1918–1923.

(21) Woessner, G.; Goeller, G.; Rieker, J.; Hoier, H.; Stezowski, J. J.; Daltrozzo, E.; Neureiter, M.; Kramer, H. E. A. *J. Phys. Chem.* **1985**, *3629*–3636.

Table 1. TD-DFT and CASSCF Vertical Excitation Energies for BZT1 and BZT2 Systems^a

excited state	BZT1 TD-B3LYP	BZT2 TD-B3LYP	BZT2 CASSCF(14,12)
S ₁	3.60 eV (expt. 3.6 eV) (0.2830) ($\pi\pi^*$, CT ₁ ^b)	4.18 eV (0.1712) ($\pi\pi^*$, CT ₁ ^b)	4.79 eV ($\pi\pi^*$, LE _{Ph} ^d)
S ₂	4.20 eV (expt. 4.1 eV) (0.1322) ($\pi\pi^*$, LE _{Tri} ^c)	4.89 eV (0.2111) ($\pi\pi^*$, CT ₂ ^e)	5.94 eV ($\pi\pi^*$, CT ₁) ^g
S ₃	4.26 eV (expt. 4.1 eV) (0.2382) ($\pi\pi^*$, CT ₂ ^e)	5.53 eV (0.0375) ($\pi\pi^*$, LE _{Ph} ^d)	7.26 eV ($\pi\pi^*$) ^h
S ₄	5.20 eV (0.0185) ($\pi\pi^*$, LE _{Ph} ^d)	5.93 eV (0.0001) ($n\pi^*$)	
S ₅	5.30 eV (0.0002) ($n\pi^*$)	S ₆ 6.37 eV (0.0321) ($\pi\pi^*$, LE _{Tri} ^c)	5.67 eV ($n\pi^*$) ^f

^a Oscillator strengths and characterization of the states in brackets; experimental values given in brackets where available; 6-31G* basis used in all computations. ^b Charge-transfer state 1, excitation from highest occupied MO on phenol moiety to lowest unoccupied MO on triazole moiety, see main text for details. ^c Locally excited state (triazole moiety). ^d Locally excited state (phenol moiety). ^e Charge-transfer state 2, excitation from second highest occupied MO on phenol moiety to lowest unoccupied MO on triazole moiety, see main text for details. ^f (16,13) CASSCF active space so cannot be compared with the energies of the $\pi\pi^*$ states. ^g This state is difficult to characterize in the FC region, however it is clearly the charge-transfer state, CT₁ at the optimized geometry and this is the designation used here. ^h A strongly mixed state that can only be designated as $\pi\pi^*$.

We now turn to the comparison of the TD-DFT results of BZT1 and BZT2. Note that analysis of the TD-DFT results for BZT1 and BZT2 is not unambiguous because there is considerable configurational mixing (e.g., the near degenerate LE_{Tri} and CT₂ states in BZT1). Comparing columns 2 (BZT1) and 3 (BZT2) of Table 1 one can see that the major difference is that the LE_{Tri} state for BZT2 is displaced to very high energies. This is obviously a consequence of the elimination of the benzo-fused substituent of BZT1. Thus our calculations on BZT2 effectively ignore the LE_{Tri} state of BZT1. However, there is no experimental evidence suggesting a role of that state in the photochemistry and photophysics of BZT1 and its derivatives. Thus the omission of the LE_{Tri} should not affect the conclusions of our study and the TD-DFT results suggest that BZT2 is a good model for BZT1.

The CASSCF results (column 4 in Table 1) for BZT2 differ significantly from the TD-DFT results: for BZT2 the lowest excited state is LE_{Ph}, and the CT₁ state now S₂. However it is well-known that CASSCF overestimates the excitation energy to ionic-type or charge-transfer states such as CT₁ and CT₂ here, and it is necessary to include dynamic correlation to correct this behavior.^{22,23} Further, as we will discuss later the chemical nature of S₂ is ambiguous (in the CASSCF computations) at the FC geometry because of configurational and orbital mixing. Indeed, analysis of the wave function at the FC region (presented later in the manuscript) shows that the amount of charge-transferred during the vertical excitation is smaller in the CASSCF computation than at the TD-DFT level. However, the most important point is that these CASSCF states correlate with two distinct S₁ minima that can be fully characterized as LE_{Ph} or CT₁ from a VB analysis. At the nonplanar CT₁ minimum, the negative charge density accumulated on the triazole moiety through the excitation is stabilized partially by an internal hydrogen bond, and this appears to improve the CASSCF description of the CT state (cf. the previous TRP study).⁸ Therefore, the rest of the ESIPT coordinate should be qualitatively correct at the CASSCF level.

To summarize: Comparison with TD-DFT results for BZT1 and BZT2 (Table 1) suggests that BZT2 is a good model. The higher energy of the LE_{Tri} state for BZT2 is just a consequence of the elimination of the benzo-fused substituent of BZT1. Thus our calculations do not consider the LE_{Tri} state of BZT1. Comparison of TD-DFT and CASSCF results for BZT2 shows that relative energies of pathways involving the LE_{Ph} and the CT₁ states in the region of enol-like geometries cannot be compared at the CASSCF level. Nevertheless, all computations agree on the chemical nature of the two lowest energy $\pi\pi^*$ states in the FC region, and the fact that the $n\pi^*$ state lies higher in energy in this region.

Choice of Active Spaces for the Reaction Path Studies. The excited state reactivity of BZT2 has been studied using a complete active space self-consistent field (CASSCF) formalism. To correctly describe the ground and $\pi\pi^*$ excited states requires an active space of 14 electrons in 12 active orbitals i.e., the 14 π -electrons are distributed in all possible ways in the 12 p _{π} molecular orbitals (see Table 2 – CAS1 space). This generates 314 028 configurations and geometry optimizations are only just feasible with this size of CI problem, but are very computationally demanding.

We have used the full CAS(14,12) π -electron active space for two purposes, (1) as a calibration for less expensive reduced active space CASSCF computations (discussed subsequently), and (2) to obtain a detailed understanding of bonding in the ground and lowest lying $\pi\pi^*$ excited states by means of the spin-exchange density matrix elements (see subsequent discussion), which can only be obtained with such a large active space.

As mentioned above, geometry optimizations are only just feasible using the full CAS(14,12) π -electron active space; however, they are computationally expensive and alternative strategies for exploring the whole excited-state potential surfaces must be sought since the $n\pi^*$ state must be included with a balanced level of accuracy. Thus our strategy has been to reduce the CAS(14,12) π -electron active space as much as possible without loss in accuracy, and also including any orbitals needed to correctly describe the $n\pi^*$ excited-states.

The size of active space needed to fully describe the $n\pi^*$ excited state is CAS(16,13) (see Table 2 – CAS2 space). This active space includes the CAS1 π -space plus the n -orbital. This generates 828 828 configurations. Single-point energy computation with this number of configurations is only possible by running the calculation in parallel over several processors. Again, this active space was used to obtain the spin-exchange density for this excited-state.

Both the above-mentioned active spaces are prohibitively large for the general exploration of the excited-state potential surfaces and the computation of their nonadiabatic couplings. Removing quasi-inactive and quasi-virtual orbitals reduced the number of configurations. The choice of quasi-inactive and quasi-virtual orbitals was made by examining the one-electron density matrix from a large active space single-point calculation. The vertical excitations for various choices of reduced active space are given in Table 2. In all states the oxygen π -orbital has an occupation number of 1.999 and can thus be removed from the active space. The removal of this orbital from the CAS2 space gives the CAS3 space in Table 2. Removal of a further quasi-inactive orbital gives a CAS(12,11) (CAS4 in Table 2), generating 106 953 configurations. This is still quite large but was used for some of the nonplanar optimizations when the choice of further orbitals to remove was not obvious. For analytical frequency computation however, a further reduction is necessary. It was generally found that a CAS(10,8) active space could be obtained which gave faithful potential energy surfaces. This generates 1176 configurations, a CI problem which is amenable to general geometry optimization and analytical frequency computation. A different CAS(10,8) space was used for $\pi\pi^*$ (CAS5 – Table 2) and $n\pi^*$ (CAS6 – Table 2) states.

Also included in Table 2 are some vertical excitations obtained from a RASSCF computation (see ref 23 for technical details). In a RASSCF computation the active orbital space is divided into three subspaces RASI, RASII, and RASIII. One does a multireference CI computation

(22) Serrano-Andrés, L.; Roos, B. *J. Am. Chem. Soc.* **1996**, *118*, 185–195.
(23) Klene, M.; Robb, M. A.; Blancafort, L.; Frisch, M. J. *J. Chem. Phys.* **2003**, *119*, 713–729.

Table 2. Vertical Excitation Energies of BZT2 for Various Choices of Active Space^a

excited state	TD-B3LYP	CAS(14,12)	CAS(16,13)	CAS(14,12)		CAS(10,8)	CAS(10,8)	RAS
		full π -space (CAS1)	full $n\pi^*$ space (CAS2)	$0\pi \rightarrow nN$ (CAS3)	CAS(12,11) (CAS4)	reduced π -space (CAS5)	reduced $n\pi^*$ space (CAS6)	
$\pi\pi^*$ LE intraphenyl	5.53 eV (0.0375)	4.79 eV		4.81 eV	4.82 eV	4.86 eV		4.87 eV
$\pi\pi^*$ CT Ph \rightarrow triazole	4.18 eV (0.1712)	5.94 eV		5.91 eV	6.01 eV	6.44 eV		5.88 eV
$\pi\pi^*$ CT Ph \rightarrow triazole	4.89 eV (0.2111)	7.26 eV		-	7.30 eV			6.94 eV
$n\pi^*$	5.93 eV (0.0001)	-	5.67 eV	5.65 eV			5.77 eV	

^a 6-31G* basis used in all computations.

using a full CI RASII space as the reference space i.e., a low dimension CAS space. In the RASI the level of excitation is limited to h (the number of holes) and the RASIII space has a maximum occupancy of e (electrons) so the computation is denoted $(n, m^I + m^{II} + m^{III})[h,e]$ where n is the number of electrons and $m^I + m^{II} + m^{III} = m$ the number of orbitals. After some experimentation, we used a (14, 5 + 5 + 2)-[1,1] space (i.e., all single excitations from a CAS(7,5) reference space). Thus, the RASSCF computations have the same size active space, CAS-(14,12), as the benchmark active spaces CAS1 and CAS3 (Table 2), but the size of the configuration space is reduced from 314 028 to 2115. This choice of RAS space was based on an inspection of the density matrixes for the relevant excited-states and removing the “passive orbitals” (the orbitals that have near 2.0 or 0.0 occupancy in all states i.e., the quasi-inactive and quasi-virtual orbitals) to RASI or RASIII spaces. Thus, the RASSCF calculations reintroduce those orbitals discarded in the reduced active space (CAS5 and CAS6 in Tables 2 and 3) computations but still keep the number of configurations manageable. The RASSCF computation serves two purposes in our study: (1) calibration of the CAS5 and CAS6 active spaces used for geometry optimization and analytical frequency computation and (2) checking the proximity of $\pi\pi^*$ states along the computed $n\pi^*$ excited-state reaction path.

Details of Wave Function Analysis and Reaction Path Calculations. The bonding in the excited-states computed with the CAS1 and CAS2 active spaces was analyzed using the spin-exchange density (P_{ij})²⁴ with localized active orbitals obtained with the Boys method.²⁵ This also provides the localized one-electron density matrix (D_{ij}).

The P_{ij} matrix elements have a simple interpretation that helps one to understand the spin coupling (see ref 26 for a thorough discussion and ref 27 for a recent example of the use of P_{ij} 's in determining excited state bonding). For a single configuration perfectly paired valence bond (VB) wave function the P_{ij} have values of +1 for a singlet-coupled pair, -1 for a triplet coupled pair and -1/2 when the pair is uncoupled. Configuration interaction will cause the actual computed values to differ from these idealized values and it is common to take a positive P_{ij} as singlet coupled and a negative P_{ij} as uncoupled. From a practical point of view, the P_{ij} elements for neighboring atoms give an idea of the π bonding, i.e., π bond localization in the different structures. For aromatic molecules, the P_{ij} values are smaller than one (cf., the reference value of approximately 0.34 in benzene).²⁶ Changes with respect to the ground-state can be understood as decrease or increase in the bond-order due to the excitation. Finally, the diagonal elements of the one-electron density matrix D_{ii} , calculated with localized active-space orbitals, give the occupations of the π orbitals and are useful to assess the charge-transfer character of the states.

To determine the ground-state reaction channels (from the conical intersection on the right-hand side of Figure 2), and also to determine the topology of the conical intersection we have used the IRD method.²⁸ For a photochemical reaction we have extended the intrinsic reaction

Table 3. (a) CASSCF Absolute Energetics^{a,b} (b) CASSCF Relative Energetics along ESIPT Deactivation Pathway^c

(a)			
geometry	adiabatic state	active space	energy (au)
enol (planar)	S_0 - minimum	(10,8) s.p.	-545.22159
		(14,12)	-545.31638
	S_1 ($\pi\pi^*$ LE phenyl) - VE	(10,8)	-545.07026
		(14,12)	-545.13632
$\pi\pi^*$ (LE)/ $\pi\pi^*$ (CT) conical intersection	S_2 ($\pi\pi^*$ CT) - VE	(10,8)	-545.01245
		(14,12)	-545.09436
	S_n ($n\pi^*$) - VE	(14,12)	-545.08396
	S_1/S_2	(10,8)	-545.02827
$\pi\pi^*$ (LE) planar minimum	S_1	(12,11)	-545.08931
		(14,12)	-545.14630
$\pi\pi^*$ (CT) nonplanar minimum	S_1	(10,8)	-545.05820
		(14,12) s.p.	-545.10587
$\pi\pi^*$ (CT)/ $n\pi^*$ avoided crossing transition state	S_1	(10,8)	-545.05479
		(10,8)	-545.02596
$n\pi^*$ planar enol minimum	S_1 (constrained A'')	(10,8)	-545.02596
		(10,8)	-545.04817
$n\pi^*$ planar keto minimum	S_1 (constrained A'')	(10,8)	-545.01422
		(10,8)	-545.01422
keto minimum (nonplanar)	S_1	(12,11)	-545.17340
		(10,8) s.p.	-545.06817
GS/ $n\pi^*$ conical intersection	S_0/S_1	(12,11)	-545.16261
		(10,8)	-545.04061
channel 3 like conical intersection	S_0/S_1	(10,8)	-545.04061

(b)		
geometry	state	relative energy to S_0 minimum/(kcal mol ⁻¹)
enol (planar)	S_0 - minimum	0.0
	S_1 $\pi\pi^*$ (LE)	113.0 ^d
	S_2 $\pi\pi^*$ (CT)	139.3 ^d
$\pi\pi^*$ (LE)/ $\pi\pi^*$ (CT) conical intersection	S_1/S_2	121.3 ^e
$\pi\pi^*$ (LE) planar minimum	S_1	106.7 ^d
$\pi\pi^*$ (CT) nonplanar enol minimum	S_1	132.1 ^d
$\pi\pi^*$ (CT)/ $n\pi^*$ avoided crossing	S_1	134.3 ^f

^a All energies at optimized geometries unless stated. ^b 6-31G* basis used in all computations. ^c 6-31G* basis used in all computations. ^d (14,12) $\pi\pi^*$ active space. ^e (10,8) $\pi\pi^*$ active space. ^f (10,8) $n\pi^*$ active space. ^g (12,11) $n\pi^*$ active space.

coordinate. This involves the computation of an initial relaxation direction (IRD), which is a minimum on an $n-1$ -dimensional hyperspherical cross-section of the potential energy hypersurface, where the search is carried out in a subspace orthogonal to a vector centered at the conical intersection. In our studies, the search vectors used were the gradient difference and derivative coupling vectors. At a sloped

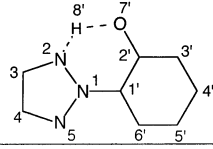
(24) Bernardi, F.; Celani, P.; Olivucci, M.; Robb, M. A.; Suzzi-Valli, G. *J. Am. Chem. Soc.* **1995**, *117*, 10 531–10 536.

(25) Boys, S. F. *Rev. Mod. Phys.* **1960**, *32*, 296.

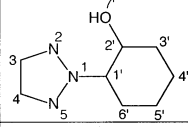
(26) Blancafort, L.; Celani, P.; Bearpark, M. J.; Robb, M. A. *Theo. Chem. Acc.* **2003**, *110*, 92–99.

(27) Paterson, M. J.; Blancafort, L.; Wilsey, S.; Robb, M. A. *J. Phys. Chem. A.* **2002**, *106*, 11 431–11 439.

(28) Celani, P.; Robb, M. A.; Garavelli, M.; Bernardi, F.; Olivucci, M. *Chem. Phys. Lett.* **1995**, *243*, 1–8.

Table 4. Fully Optimized Geometries, See Figure 2 (all bond lengths in Ångströms)


	S_0	$\pi\pi^*$ LE _{Ph}	S_1 CT ₁ enol minimum	S_1 CT ₁ transition state	$S_1 n\pi^*$ keto minimum	S_0/S_1 conical intersection
1 - 2	1.34	1.31	1.44	1.42	1.47	1.41
2 - 3	1.34	1.31	1.33	1.33	1.46	1.39
3 - 4	1.40	1.39	1.39	1.38	1.32	1.39
4 - 5	1.34	1.31	1.31	1.31	1.46	1.32
1 - 5	1.34	1.31	1.43	1.41	1.43	1.39
1 - 1'	1.43	1.40	1.37	1.40	1.45	1.42
1' - 2'	1.41	1.45	1.44	1.45	1.42	1.41
2' - 3'	1.40	1.43	1.43	1.44	1.42	1.40
3' - 4'	1.39	1.43	1.36	1.37	1.39	1.40
4' - 5'	1.40	1.42	1.44	1.43	1.41	1.39
5' - 6'	1.39	1.43	1.37	1.40	1.39	1.39
1' - 6'	1.40	1.43	1.43	1.35	1.42	1.39
2' - 7'	1.35	1.34	1.29	1.26	1.41	1.34
2 - 8'	1.92	1.80	1.68	1.43	1.05	1.04
7 - 8'	0.95	0.99	0.99	1.08	2.50	3.27
(2' - 1' - 1 - 5) dihedral angle	180.0°	180.0°	166.0°	163.7°	-170.1°	-102.7°

Table 5. Localized One-Electron Density Matrix Elements (D_{ij})


	S_0	$\pi\pi^*$ LE _{Ph} Minimum	$\pi\pi^*$ CT ₁ (S_2 Vertical)	$\pi\pi^*$ CT ₁ Minimum	$S_1 n\pi^*$ keto
1	1.50	1.47	1.49	1.56	1.79
2	1.24	1.27	1.35	1.33	1.82
3	1.02	1.02	0.98	1.01	1.04
4	1.03	1.04	0.98	1.09	0.98
5	1.19	1.21	1.29	1.52	1.35
1'	1.08	1.08	1.05	0.70	0.99
2'	0.97	0.97	0.98	1.09	0.98
3'	1.03	1.05	1.02	0.94	0.99
4'	0.99	1.02	0.97	0.96	1.00
5'	1.02	0.97	1.03	1.05	0.99
6'	1.00	1.04	0.96	0.78	0.99
7'	1.92	1.87	1.90	1.99	π - 1.14 n - 1.94

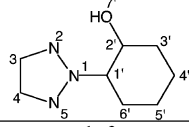
conical intersection, very similar IRDs should be found even when using two orthogonal search directions, since there is only one relaxation channel. The gradients at the IRD's can also be examined in order to verify that only one relaxation channel exists.

Results and Discussion

Chemical Characterization of the $\pi\pi^*$ and $n\pi^*$ excited states. We begin our discussion with a VB analysis of the various excited states using the P_{ij} analysis presented in the computational details section. Looking at the change in the bonding patterns from ground and excited states, one may rationalize the initial geometry relaxations following photoexcitation. Optimized geometries are collected in Table 4, localized one-electron density matrix elements (D_{ij}) are collected in Table 5 and spin-exchange density matrix elements (P_{ij}) are collected in Table 6.

The ground state of the BZT2 molecule has the predicted resonance structure shown in Scheme 1. The optimized geometry of the S_0 minimum, given in Table 4, has bond lengths consistent with this and the nature of the electronic state can be confirmed by an inspection of the P_{ij} indices shown in Table 6.

The vertically excited states of BZT2 have been calibrated against those of the BZT1 using time-dependent density functional theory (TD-DFT) as shown in Table 1 and discussed previously in the computational details section. We now discuss

Table 6. Spin-Exchange Density Matrix Elements (P_{ij})


	S_0	$\pi\pi^*$ LE _{Ph}	$\pi\pi^*$ CT ₁ (S_2 Vertical)	$S_1 \pi\pi^*$ CT ₁ enol	$S_1 n\pi^*$ keto
1 - 2	0.149	0.145	0.098	0.009	0.016
2 - 3	0.370	0.351	0.244	0.193	0.001
3 - 4	0.275	0.276	0.153	0.233	0.366
4 - 5	0.397	0.296	0.276	0.350	0.419
1 - 5	0.166	0.163	0.014	0.021	0.420
1 - 1'	0.043	0.081	0.105	0.278	0.002
1' - 2'	0.297	0.163	0.213	0.032	0.241
2' - 3'	0.292	0.227	0.294	0.166	0.265
3' - 4'	0.356	0.257	0.322	0.477	0.356
4' - 5'	0.312	0.288	0.268	0.128	0.334
5' - 6'	0.355	0.248	0.372	0.474	0.312
1' - 6'	0.296	0.236	0.196	0.088	0.377
2' - 7'	0.038	0.043	0.048	0.048	0.268

the bonding in these states. The chemical nature of the lowest energy $n\pi^*$ state is excitation from the antisymmetric combination of nitrogen lone pair orbitals to the π^* LUMO as shown in Figure 4. This changes to excitation from the oxygen in-plane lone pair orbital along the ESIPT path, leading to an avoided crossing transition state between the two diabatic states (Figure 4c). The $\pi\pi^*$ excited states require a more detailed discussion.

The lowest lying excited states of the enol form at the CASSCF level are $\pi\pi^*$ excited states. The localized one-electron densities (D_{ij}) for the ground, $\pi\pi^*$ (LE_{Ph}) and $\pi\pi^*$ (CT₁) states are given in Table 5, whereas the spin-exchange density matrix elements (P_{ij}) for the $\pi\pi^*$ excited states are given in Table 6. From this analysis, one obtains the resonance forms in Figure 3.

The first excited state, S_1 , can be unambiguously assigned as LE_{Ph} at the CASSCF level (see Tables 4–6, and Figure 3), i.e., local excitation on the phenyl group. Wave function analysis at the Franck–Condon geometry and the optimized planar minimum gives the same results, and only the P_{ij} and D_{ij} elements at the minimum are given. This excitation is similar to the $S_0 \rightarrow S_1$ excitation of benzene as is evident from the reduction in the P_{ij} values. The spin-couplings on the triazole are unaffected by the S_1 excitation, whereas those on the phenyl group are reduced analogously to the S_1 excitation in benzene

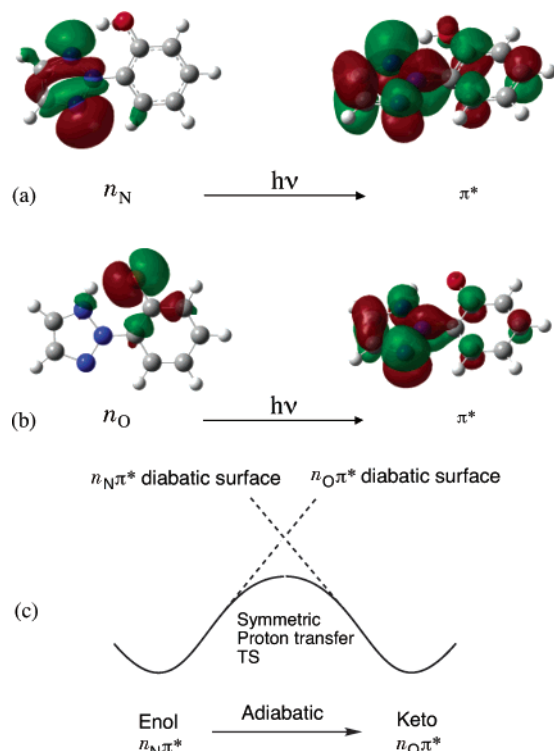


Figure 4. Orbital representation of the $n\pi^*$ state. (a) Enol geometries ($n_N\pi^*$). (b) Keto geometries ($n_O\pi^*$). (c) Schematic of the adiabatic $n\pi^*$ surface along the proton-transfer coordinate for planar geometries.

i.e., the Kekulé to anti-Kekulé transition. Relaxation of the LE_{Ph} state leads to a planar minimum (optimized with the CAS1 space), with C_s symmetry and geometrical changes localized on the phenyl group, consistent with the locally excited nature of this state. This geometry is given in Table 4. The main geometrical changes are elongated CC bonds in the phenyl group, consistent with the reduced spin-coupling between the π -electrons in the LE_{Ph} state. The fact that this planar geometry is a minimum has been verified by means of an analytical frequency calculation using the geometry in Table 4 with the CAS5 active space.

The analysis of S_2 at the CASSCF level is less conclusive at the FC geometry (Table 6). In the dominant configuration the excitation goes from an MO delocalized over the whole molecule to one that is localized on the triazole unit. Partial charge-transfer character is obtained by summing the diagonal one-electron density matrix elements for localized orbitals D_{ii} (see the Computational Details) for both moieties (Table 5). This gives a small charge-transfer character of 0.1 electrons. However, we are able to correlate this vertically excited state with the charge-transfer state minimum on the S_1 adiabatic surface. At the minimum for the CT state the charge-transfer character is more pronounced due to the folded geometry. This identifies the state as responsible for the proton-transfer reactivity.

Idealized Planar Reaction Path Coordinate (Figure 1). We now discuss the computed proton-transfer reaction path, under constraint of planarity, for the $n\pi^*$ excited state. As discussed above, the absorbing state is a $\pi\pi^*$ state and the $n\pi^*$ state lies at higher energy. This is the case for all planar geometries. Thus there is no possibility of radiationless deactivation to the ground

state along this path. Nevertheless this reaction path is a useful reference point.

We have optimized points along the proton-transfer coordinate constrained to planar geometries using the CAS5 active space discussed above (see Figure 4). At planar geometries, there exists an enol critical point on the $n\pi^*$ surface, which is a first-order saddle-point in the full space of coordinates. The optimized geometries along the planar reaction path are given in Supporting Information, and the energetics are collected in Table 3a,b. The transition state geometry has the proton equidistant (1.24 Å) between the nitrogen and the oxygen. In the full space of nuclear coordinates the planar geometry is in fact a third order saddle-point. Although the largest imaginary frequency corresponds to the proton transfer coordinate, the other two imaginary frequencies are associated with out of plane deformations. Note that the analytical frequency computation is performed without any symmetry constraints. Thus, the physically relevant reaction path will lie at folded and twisted geometries to be discussed subsequently.

A planar keto critical point also exists on the $n\pi^*$ excited state. As expected this is not a minimum in the full space of coordinates but rather a saddle-point. The imaginary frequency is associated with out of plane bending indicating a lower energy folded geometry.

At the planar geometries just discussed, RASSCF computations show that the $n\pi^*$ state is not the lowest excited state, but that a $\pi\pi^*$ state is always lower in energy. Thus, the out of plane proton transfer reaction path is not only much lower in energy than the planar coordinate, but as we shall discuss the nonplanar reaction path leads to a conical intersection which is ultimately responsible for the radiationless decay.

Path A—Nonplanar ESIPT Reaction Path (Figure 2). The nonplanar ESIPT reaction, that provides the radiationless decay path, starts at a nonplanar minimum of the CT $\pi\pi^*$ state. The geometries along the nonplanar reaction path are given in Table 4. Tables 5 and 6 give the diagonal one-electron density and the spin-exchange elements (D_{ii} and P_{ij} elements, respectively; see the Computational Details) for these structures. From the sum of the D_{ii} elements on the two parts of the molecule, 0.5 electrons are transferred from the phenol to the triazole moiety. Comparison of the D_{ii} elements of the present structure with the ones for the ground-state at the FC geometry (Table 5) shows that the positive charge density is localized on the $C_{1'}$ and $C_{6'}$ phenol carbons, whereas the negative charge density is localized on the N_2 and N_5 triazole nitrogen atoms (see atom numbering in Tables 4–6). Further analysis of the P_{ij} values and the bond lengths gives no clear-cut picture of the bonding at the nonplanar enol minimum, and this structure is therefore characterized loosely with the resonance structures of Figures 3c and 5, which signify the charge-transfer between the two aromatic rings. In any case, the essential point is that the charge-transfer results in the formation of an intramolecular bond between the hydrogen atom of the hydroxy group and the nitrogen that accepts the proton. This is evident from the shortening of the corresponding distance from 1.79 Å at the FC geometry to 1.68 Å at the nonplanar minimum. The remainder of the ESIPT path goes through an avoided crossing transition state that separates the enol and keto structures on S_1 . This transition state for the excited-state intramolecular proton transfer is on the S_1 adiabatic

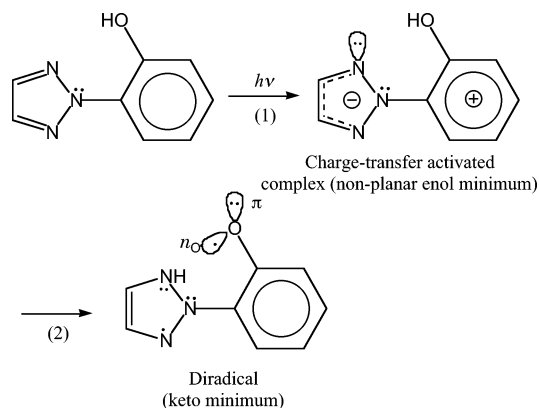


Figure 5. Rationalization of the coupled electron and proton-transfer mechanism. (1) Photoinduced formation of charge-transfer activated complex. (2) Proton transfer from the activated complex.

state and leads to the excited-state minimum of the keto tautomer, as determined by a forward IRC calculation.

The geometry for the nonplanar proton-transfer transition state is given in Table 4. It is clear that the transition state geometry lies on the enol side of the reaction, and will be encountered after the state switch between the $\pi\pi^*$ and $n\pi^*$ excited states which must occur at enol geometries. The reaction path from the transition state leads to a nonplanar excited-state keto minimum some 12.0 kcal mol⁻¹ lower in energy (see Table 3a,b). At this geometry the energies of the S_1 and S_0 states are reasonably close in energy, so state-averaged orbitals were used for geometry optimization and subsequent analytical frequency calculation.

We now discuss the nature of the S_1 state at the keto minimum shown in Table 4 and Figure 5. The electronic state is a diradical-like open-shell state, which reflects the fact that the hydrogen transfer is a coupled proton and electron transfer, with respect to the ground state at the FC geometry. This can be understood by counting the electrons (sum of the D_{ii} elements) involved in the process, namely the π system and two in-plane electron pairs. Thus, the initial ground-state structure has 8 electrons on the triazole moiety (6 π electrons and the nitrogen lone pair) and 10 on the phenol moiety (8 π electrons and the σ O–H bond). The excited-state keto tautomer has 9 electrons on the triazole unit (7 π electrons and the new σ N–H bond) and 9 on the phenyl part (8 π electrons and one in the n_O orbital), and the overall process is a hydrogen atom transfer (electron plus proton). Thus, the proton-transfer compensates the transfer of the electron and leaves an overall biradical. On the basis of the P_{ij} values of Table 6, the structure of the phenol moiety corresponds to the ($n\pi^*$) excited state of a phenoxy radical which is essentially located on the oxygen atom, whereas the phenyl ring remains largely aromatic (see the small differences in the P_{ij} elements and the bond lengths in the phenyl ring, between the present structure and the ground state at the FC geometry). Interestingly, then, the electronic structure of the keto intermediate does not correspond to a bona fide ketone, although the use of the label is justified to distinguish the tautomeric form from the enol one. As for the triazole unit, the bond lengths indicate the formation of a bond between the C_3 and C_4 atoms, as shown in Figure 5. However, the high P_{ij} values for the adjacent C_4 – N_5 and N_5 – N_1 bonds indicate that the radical is substantially delocalized over the ring.

The overall hydrogen transfer can be rationalized in two steps (Figure 5), in analogy to the same process in tryptophan (TRP).⁸ In TRP, the $^1\pi\pi^*$ fluorescence is quenched by an excited-state proton transfer in which the first step is the formation of the activated complex. This occurs after a state switch between the 1L_b (covalent) and the 1L_a (ionic) states, and the ionic state provides the first driving force for the hydrogen transfer. In the BZT case the state that triggers the H transfer is the charge-transfer state, and the first step is the formation of the activated complex (the nonplanar enol minimum). The next step in the TRP decay is the coupled electron and proton transfer from the donor to the indole ring. In BZT, the next step is the proton transfer from the hydroxy group to the triazole, that compensates the previous transfer of a negative charge, as discussed above on the basis of the D_{ii} elements of the keto intermediate. Together with the proton transfer there is an electronic rearrangement in the phenoxy moiety that yields the phenoxy radical structure of the keto minimum. Overall, the hydrogen transfer is different in the TRP and BZT cases because in TRP the ionic state that triggers the proton transfer does not involve, in first instance, a charge-transfer from the proton donor to the acceptor. In contrast, in BZT the phenol moiety acts first as electron and then as proton donor, and the mechanism resembles the one described for coupled proton and electron transfer in the excited-state tautomerization of the guanosine–cytosine base pair²⁹ and a 2-aminopyridine dimer analogue.³⁰ We note that the coupled electron and proton transfer could be understood to be sequential. However, the separation of the overall process in single steps is only formal (only 0.5 electrons are transferred to the triazole moiety during the formation of the nonplanar enol minimum, while the rest of the charge-transfer takes place during the proton transfer), and we therefore speak of a coupled process.

Our discussion now returns to the keto side of the reaction path i.e., the forward IRC from the transition state given in Table 4. Very close to the keto minimum, there exists a conical intersection between the S_0 and S_1 states (approximately 7 kcal mol⁻¹ above the minimum). The optimized geometry is given in Table 4 and Figure 6a, whereas the coordinates defining the “branching space” which lift the degeneracy are shown in Figure 6b,c. The branching space is spanned by the gradient difference and derivative coupling vectors, which are the coordinates that lift the degeneracy of the two states at first order i.e., for infinitesimal nuclear motion. These coordinates can be seen to mainly involve CO and NH stretching. This is consistent with the regeneration of the ground-state enol form. In addition there is motion on the central pyramidalized nitrogen, which indicates a return to a planar conformation.

The proximity of the conical intersection to the S_1 minimum provides the mechanism for the radiationless decay and therefore the photostability. This conical intersection has a sloped topology in the terminology of Ruedenberg et al.,³¹ which means that generally there exists only one reaction channel on the ground-state surface. An optimized IRD has been found on the ground and excited-state surfaces. The gradient at the optimized ground-state structure is given in Figure 7. The gradients on both S_0 and S_1 are almost parallel, which is indicative of a sloped

(29) Guallar, V.; Douhal, A.; Moreno, M.; Lluch, J. M. *J. Phys. Chem. A* **1999**, *103*, 6251–6256.

(30) Sobolewski, A. L.; Domcke, W. *Chem. Phys.* **2003**, *294*, 73–83.

(31) Atchity, G. J.; Xantheas, S. S.; Ruedenberg, K. *J. Chem. Phys.* **1991**, *95*(3), 1862–1876.

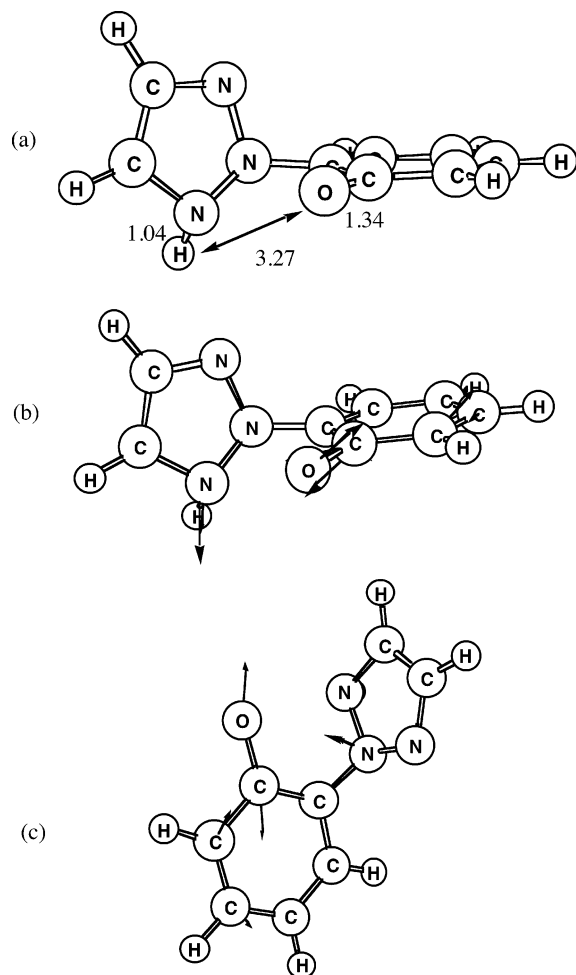


Figure 6. S_0/S_1 ($n\pi^*$) conical intersection responsible for ultrafast deactivation of excited-state species. (a) Optimized with CAS(10,8)/6-31G*. (b) Derivative coupling vector. (c) Gradient difference vector. (All bond lengths in Ångströms).

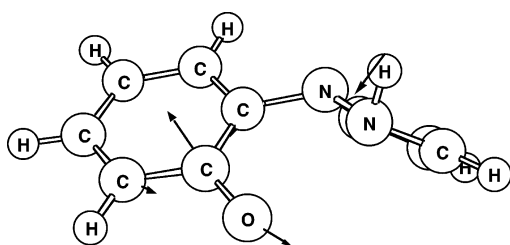


Figure 7. Gradient at optimized IRD on S_0 surface. This corresponds to the ground-state relaxation channel and involves CO and OH stretching, leading to the regeneration of the enol form. The gradient of the IRD on S_1 is very similar which is indicative of a sloped conical intersection topology.

conical intersection (see ref 27, where IRD searches have been used to determine the topology of the intersection). The gradient shown in Figure 7 involves both CO stretching and NH stretching. In our system, this corresponds to the regeneration of the ground state enol structure. In fact, at the CI the CO bond has recovered the original length of the enol, but the gradient at the IRD indicates that during the back transfer of the hydrogen atom the CO bond length undergoes further changes (presumably bond stretching and subsequent compression). We have not studied the details of this process. However, we were unable to locate any ground-state keto minima using both CASSCF and density functional theory (B3LYP) i.e., all

optimizations eventually returned to the ground state planar enol form. Thus, the lack of a stable ground state keto species, coupled to the accessible sloped conical intersection gives rise to the photostability of benzotriazoles, since the regeneration of the enol form from the excited state form is effectively a barrierless process.

Our computations show a low barrier to radiationless decay (energy difference between the keto minimum and the conical intersection of 6.7 kcal mol⁻¹, Table 3a,b). The low barrier agrees qualitatively with the short lifetimes of the experimentally observed long-wavelength intermediate.²⁰ However more quantitative conclusions (for example about the different lifetimes obtained for different derivatives of BZT1) are not possible because the calculations lack dynamic correlation.

Points on the seam of degeneracy may exist all along the proton transfer path and the molecule may decay to the ground state at any of these points and need not fully react to the keto form in order to undergo radiationless deactivation. We have optimized a point on this seam by minimizing the S_0/S_1 energy difference, starting from the S_1 CT enol minimum geometry given in Table 4. In this way, the nearest point of degeneracy is found (the geometry is given in Supporting Information). The NH distance at this point is 1.49 Å, whereas the OH bond length is 1.06 Å. Thus, while we could not find an optimized point of intersection on the enol side, the fact that the seam of intersection exists all along the proton transfer path is demonstrated. The seam will only be relevant if the adiabatic S_1 state wave function has enough $n_0\pi^*$ character, since this is the relevant crossing state. However, we have demonstrated that the switch to that state occurs quite early along the reaction path (the TS is already $n_0\pi^*$). Thus, the system could decay at any point along this seam, and dynamical simulations would be required to determine the most probable hop locations along the seam. The resulting process can be seen as a variant of the “aborted” hydrogen transfer at a conical intersection found for a diaza compound in dichloromethane,³² that was recently proposed as a possible mechanism for the ESIPT in BZT.⁵

Path B—Possible Stabilization and Photodegradation Pathway from S_1 (LE Benzene-like State). The next point of the discussion concerns an alternative photodegradation pathway which may be responsible for the behavior of BZT and its derivatives as photostabilizers over a long time scale. This pathway involves the locally excited, benzene like LE_{Ph} state, and deactivation can lead to regeneration of the reactant (i.e., photostabilization) or rearrangement of the benzene skeleton and subsequent photodegradation. The pathway goes through the planar minimum of the enol tautomer characterized as LE_{Ph} (see above), which lies 6.3 kcal mol⁻¹ below the vertical excitation of that state (S_1 at the CASSCF level). The decay occurs at a conical intersection that has a prefulvene geometry and was optimized using the CAS1 active space discussed previously (see Figure 8). The intersection is an analogue of the one found in the well-known channel 3 of benzene photochemistry.^{33–37} It has the characteristic three-carbon kink on the phenyl group and can regenerate benzene or yield a valence isomer (prefulvene) in its ground state.

The quantum yield of photochemical products from the channel 3 decay is very small (~ 0.02),³⁷ but this alternative

(32) Sinicropi, A.; Pogni, R.; Basosi, R.; Robb, M. A.; Gramlich, G.; Nau, W. M.; Olivucci, M. *Angew. Chem., Int. Ed.* **1998**, *37*, 98–101.

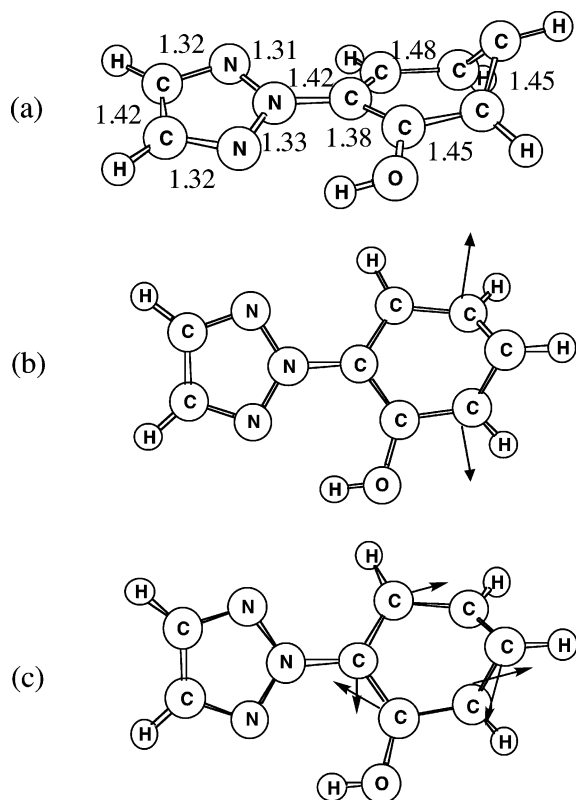


Figure 8. CAS(14,12)/6-31G* optimized S_0/S_1 conical intersection. (a) The geometry of the phenyl group is very similar to the benzene channel 3 S_0/S_1 conical intersection. This intersection leads to ultrafast decay from the S_1 locally excited phenyl state. (b) The gradient difference vector. (c) The derivative coupling vector. (All bond lengths in Ångströms)

pathway can be important for benzotriazoles since, as we have seen above the proton transfer decay pathway is essentially 100% efficient at regeneration of the ground-state enol species (due to the lack of a stable keto minimum on the ground state). Benzotriazoles do however show some degradation on very long time scales. Thus, although the reactive quantum yield from this decay pathway will be very small, over many photocycles the chromophore may begin to degrade. The photoproduct may form any one of a large manifold of possible products.

Initial Part of the Decay and Competition between the ESIPT and Benzene-like Channels. Our CASSCF calculations have identified two alternative pathways for radiationless decay, the ESIPT followed by folding of the protonated triazole moiety and an analogue of the benzene channel 3 decay for the phenol group. The decay paths start at two different minima on the S_1 surface, a nonplanar structure for the ESIPT path and a planar one for the benzene-type channel. However, one point that cannot be addressed in detail by our calculations concerns the access to the two channels after the excitation, i.e., the initial part of the decay. Thus, the CASSCF calculations favor the formation of the planar excited state minimum by approximately 25 kcal mol⁻¹, but this result is not significant because of the well-known tendency of CASSCF to overestimate the energy

of CT states by up to tens of kcal mol⁻¹. In any case, the predominance of the ESIPT has been well established experimentally, and it seems clear that the nonplanar ESIPT precursor should be the preferred excited state structure upon inclusion of dynamic correlation. Besides, the TD-DFT calculations on the BZT1 molecule indicate that there are three spectroscopically active states (see Table 1). Thus, the decay from the FC geometry for the locally excited S_2 and S_4 states will involve one or more nonadiabatic steps (decay through conical intersections between the excited states) and eventually adiabatic ones (passage through the planar S_1 minimum). This region of the potential energy surface cannot be studied reliably at the CASSCF level, and unfortunately higher-level methods that include dynamic correlation are not capable yet of treating a problem of such complexity and size. In this context, we note that the use of the reduced-size BZT2 model means that we are effectively ignoring one of the spectroscopic states, a local excitation on the benzotriazole moiety. In view of the results for BZT2, it is possible that a benzene-type channel is also found for the benzotriazole moiety, thus presenting a further possibility of photodegradation.

Possible Fluorescence from a TICT State of the Phenolate Anion. BZT UV absorbers in their ground electronic state exist in equilibrium between the intramolecularly hydrogen bonded closed form (discussed previously) and an open-form. The open-form does not contain an intramolecular hydrogen bond and the two rings are therefore free to twist relative to each other. Only the closed form exists in nonpolar media. The equilibrium can be shifted to the open-form if a suitably polar, hydrogen-bond accepting solvent is used, for example DMSO.³ Whereas, the closed form generally does not emit, the open-form emits in the blue at roughly 420 nm. It is believed that, under photolytic conditions, the solvent accepts the hydroxy proton of BZT to leave the phenolate anion.

We have investigated this by studying the phenolic anion of the BZT2 model discussed above. The CAS1 active space discussed above is suitable for this study because the $n\pi^*$ state no longer plays a role in the excited-state reactivity. We have located a minimum on S_1 and an adjacent conical intersection between S_1 and S_0 (shown in Figure 9), where the excitation is a charge-transfer from the phenolate anion to the triazole group. Both structures have a twisted geometry of C_s symmetry, where the rings are perpendicular to each other. Thus at these structures the excited state of the phenolate anion is a TICT state, as suggested recently on the basis of experimental results. The ground state of the anion has negligible double bond character in the central bond, and therefore the twisting is not sufficient to induce the state-degeneracy with the TICT state (i.e., the TICT state of the phenolate anion does not conform to the “biradicaloid charge-transfer model”).¹⁸ On the contrary, the decay point to the ground state is reached principally along a bond-recoupling coordinate (Figure 9). The conical intersection lies 17 kcal mol⁻¹ above the excited-state minimum, and the substantial energy barrier should account for the long lifetimes of the fluorescence in the blue region.

Conclusions

The mechanism suggested for the excited-state intramolecular proton-transfer reaction path in a model benzotriazole (BZT2) is summarized in Figure 2. The initial excitation of the enol

- (33) Bryce-Smith, D.; Gilbert, A. *Rearrangements in Ground and Excited States* Vol. 3; de Mayo, P., Ed.; 1980.
 (34) Lee, S. A.; White, M.; Noyes, W. A. *J. Chem. Phys.* **1976**, 2805.
 (35) Smith, B. R.; Bearpark, M. J.; Robb, M. A.; Bernardi F.; Olivucci, M. *Chem. Phys. Lett.* **1995**, 242, 27–32.
 (36) Palmer, I. J.; Ragazos, I. N.; Bernardi, F.; Olivucci, M.; Robb, M. A. *J. Am. Chem. Soc.* **1993**, 115, 673–682.
 (37) Kaplan, L.; Wilzbach, K. E. *J. Am. Chem. Soc.* **1968**, 90, 3291.

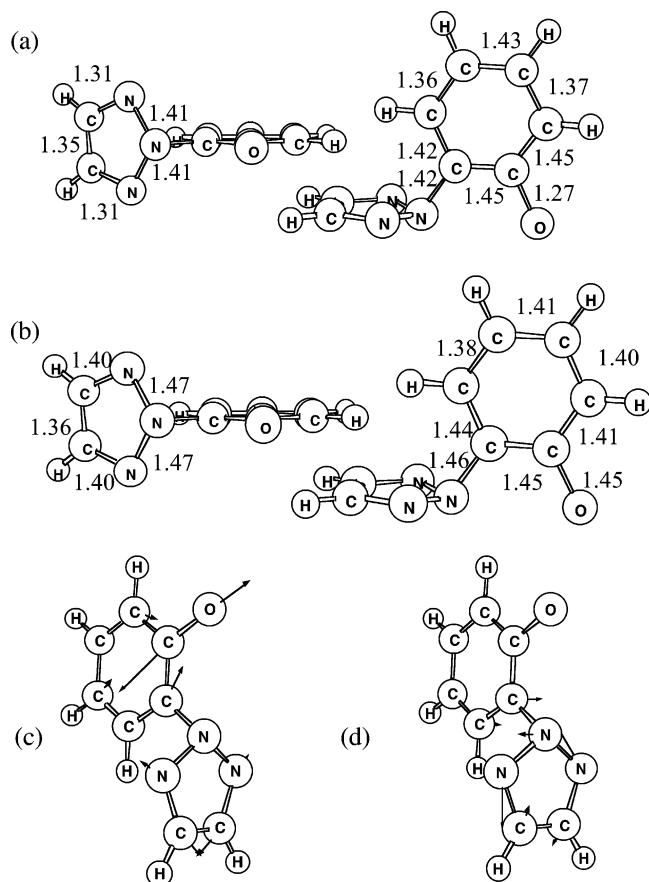


Figure 9. BZT phenolate anion. (a) CAS(14,12)/6-31G* optimized geometry of the S_1 twisted minima. (b) CAS(14,12)/6-31G* optimized geometry of the S_0/S_1 twisted intersection. (c) The gradient difference vector. (d) The derivative coupling vector. (All bond lengths in Ångströms).

form to a manifold of $\pi\pi^*$ excited states is followed by out of plane distortion and formation of an excited state complex characterized by an intramolecular hydrogen bond. This structure is a minimum of a CT state from the phenol to the triazole. The out of plane motion is essential in order to explain the ultrafast nature of the photochemical process. The ESIPT reaction proceeds adiabatically on the S_1 surface and is coupled to an asymmetric proton-transfer transition state and a switch between the CT state and an $n\pi^*$ state. The adiabatic reaction path terminates with the formation of the stable excited state keto species. A close lying conical intersection with a sloped topology is responsible for the regeneration of the ground state enol form. This entire photocycle can be completed on an ultrafast time scale, as there are effectively no barriers in the cycle.

The present results are in agreement with several previous experimental and theoretical findings about BZT1. Thus, the lowest excited state was identified as a CT state on the basis of semiempirical calculations.³⁸ The TD-DFT calculations agree with this result, and our calculated reaction mechanism highlights the importance of this state as the trigger of the radiationless decay.

(38) Catalán, J.; Fabero, F.; Guijarro, M. S.; Claramunt, R. M.; Santa María, M. D.; Foces-Foces, M. C.; Hernández Cano, F.; Elguero, J.; Sastre, R. *J. Am. Chem. Soc.* **1990**, *112*, 747–759.

The role of the charge-transfer state as a trigger of the ESIPT process suggests an explanation of unexpected experimental results on the effect of electron withdrawing groups (EWG) on the triazole unit.⁵ EWG groups improve the lifetime of the photostabilizer. It was originally thought that the key to the stabilization mechanism was the strength of the intramolecular H-bond. An EWG on the triazole pulls electron density out of the H-bond and should increase the degradation. However, this expectation is based on ground-state considerations. The excited state reactivity is dominated by formation of the charge-transfer enol minimum, precursor of the ESIPT, and an EWG on the triazole unit will favor this process by stabilizing the negative charge density in the excited state. In principle, the stabilization of the charge-transfer intermediate could also induce a decrease in the proton transfer rate by stabilization of the reactant for the second mechanistic step. However, the proton transfer step appears to be sufficiently exothermic not to be affected by the EWG, and this effect is not observed experimentally.

Moreover, the existence of the keto tautomer as a short-lived intermediate (lifetime between 500 fs and 1.2 ps) has been also established experimentally,²⁰ and vibrational coherence for low-frequency modes of 250 and 470 cm^{-1} has been observed in the decay of the keto form.³⁹ In our frequency calculation at this minimum, the pyramidalization mode of the amine nitrogen is included in low-frequency modes with uncorrected frequencies of 205 cm^{-1} and 272 cm^{-1} . Thus, our calculations are in agreement with the previous suggestion⁷ that the out of plane bending of the triazole group may be responsible for the observed vibrational coherence.

There are two alternative reaction paths that may be responsible for the photolysis of the stabilizer over many photocycles. The first one involves the $\pi\pi^*$ state localized on the phenol part and provides a photodegradation path similar to the channel 3 excited-state decay of benzene. The second alternative is a long-lived TICT state for the phenolate anion that can be generated in DMSO. A similar structure could exist for the neutral BZT form and cause photodegradation.

Acknowledgment. We are grateful to one anonymous referee for his suggestions in the interpretation of the TD-DFT results. All computations were carried out on an IBM-SP2 funded jointly by IBM-UK and HEFCE (UK). Ciba Specialty Chemicals provided financial support for this project to M. J. Paterson and M. A. Robb. L. Blancafort is financed by the Ramón y Cajal program from the Spanish Ministerio de Ciencia y Tecnología and by Grant Nos. BQU200204112-C02-02 and BZ2002-03334 from the Spanish Dirección General de Investigación (MCyT).

Supporting Information Available: The following supporting material is available: Cartesian coordinates of all optimized geometries and two quick-time movie files showing the ESIPT transition vector at symmetrical and asymmetrical transition states. This material is available free of charge via the Internet at <http://pubs.acs.org>.

JA0386593

(39) Chudoba, C.; Riedle, E.; Pfeiffer, M.; Elsaesser, T. *Chem. Phys. Lett.* **1996**, *263*, 622–628.